Ion-Sensitive Gated Bipolar Transistor (ISBiT)

R.J.E. Hueting, *Senior Member, IEEE*, S.E.J. Vincent, J.G. Bomer, R.G.P. Sanders, and W. Olthuis

***Abstract*—In this work we study the ion-sensitive gated bipolar transistor (ISBiT) by forward biasing the source-body diode of the ion-sensitive field-effect transistor (ISFET). Based on theory, extensive TCAD device simulations and experiments, it is shown that the ISBiT has a lower gate voltage operation with a higher transconductance (g_{m}) compared to the ISFET both in subthreshold and near threshold. In addition, overall maximum g_{m}'s have been obtained for the former when operating in saturation mode. However, in linear superthreshold operation mode the ISBiT shows lower g_{m}'s because of the field-induced mobility reduction. The same trends have been obtained for the pH-sensitivity expressed as $\partial I_{\mathrm{D}}/\partial \mathrm{pH}$ since it is linearly dependent on the g_{m}, as predicted by theory. Basically, the ISBiT offers more tunability hence freedom in the sensor system.**

***Index Terms*—MOS devices, Bipolar devices, sensor, ISFET, BJT**

I. Introduction

The ion-sensitive field-effect transistor, or in short the ISFET, is a potentiometric chemical transducer [1], [2]. The unmodified oxide-solution interface renders this device a pH sensor [3]- [6] and modifications result in a class of (bio)chemical sensors named ChemFETs [7]- [9]. This device is basically a field-effect transistor in which a reference electrode acting as a gate is dipped in an aqueous solution, as schematically illustrated in Fig. 1. The basic principle of the device is that the unscreened part of the ionic chemical charge in the solution is mirrored to a predictable behavior of charge in the electrical domain, the transistor. This mirror function is expressed in the transconductance (g_{m}), and relates the charge on the gate oxide-solution interface (the input) to the drain current (the output). This mirror can be improved by increasing the g_{m} as explained in section II.

One approach to increase the g_{m} is to employ a bipolar transistor that amplifies the current of the ISFET. Such approach has been reported earlier for various designs [10]- [15] showing impressive results, however most of these designs are relatively difficult to realize.

Based on an idea reported earlier [16]- [19], a so-called lateral gated bipolar junction transistor was proposed as an ion-sensitive device, that is claimed to have a relatively high g_{m} and therefore is more sensitive compared to the ISFET [20], [21]. Interestingly, the authors used specific proteins to prove their point and they used dedicated designs for improving the sensitivity. However, their analysis was general in the sense for what operating conditions such a bipolar operation mode in the ISFET offers a higher g_{m}. Moreover, the theory behind it was lacking.

The authors are with the MESA+ Institute for Nanotechnology, University of Twente, Enschede, The Netherlands.

Corresponding author: R.J.E. Hueting, University of Twente, 7500 AE Enschede, The Netherlands (email: r.j.e.hueting@utwente.nl)

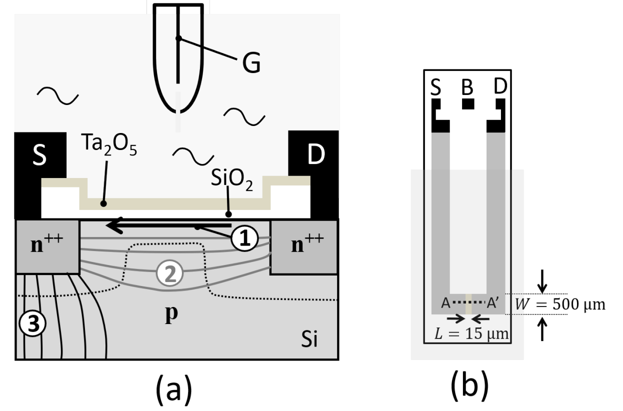

Fig. 1. (a) Schematic cross-section of a bulk ISFET. Contrary to a conventional MOSFET, the ISFET has a gate (G) electrode that has been removed and been replaced by a reference electrode and the gate oxide is in contact with an aqueous solution. The ISFET can be operated as a lateral gated bipolar transistor, *i.e.* ISBiT, when forward biasing the source-body (SB) diode (the body contact has been placed in the third dimension, as indicated in Fig. 1(b)). In addition to the increased drain current of the ISFET (1), the ISBiT has two other current components: (2) a drain (or collector) current in the body, and (3) a source (or emitter) current in the body. (b) Top view layout of the realized ISFET with a separated body or bulk contact. The gate width W = 500 μm and gate length L = 15 μm. The source/drain phosphorus peak doping concentration is $\sim 3{\cdot}10^{19}$ cm^{-3}, the source/drain-body diffused junction depth is $\sim$2.5 μm, and the boron substrate doping is $2{\cdot}10^{15}$ cm^{-3}.

In this work we report on the ion-sensitive gated bipolar transistor, *i.e.* the ISBiT, that is formed by forward biasing the source-body diode in a conventional ISFET [1]. As indicated in Fig. 1, such an ISBiT can be realized in the same technology by having a separate body (B) or bulk contact, and adopting the source (S), drain (D) as an emitter, respectively, collector.

We discuss the working principle of the ISBiT and analyze the electrical results to determine for what operating conditions the ISBiT is more attractive than the conventional ISFET for the same geometry. In addition to this analysis, TCAD device simulations and experiments have been carried out, of which the results are presented here.

II. Basic Theory

We first focus on the electrostatics of the n-type ISFET which holds for the (NPN) ISBiT as well, as explained further in this section.

Considering a 1-D capacitor configuration we can write [22], [1]:

$$\begin{aligned} V_{\mathrm{GB}} &= -\frac{Q_{\mathrm{f}}+Q_{\mathrm{it}}+Q_{\mathrm{s}}}{C_{\mathrm{ins}}}+\psi_{\mathrm{s}}+\frac{\varphi_{\mathrm{m}}-\varphi_{\mathrm{s}}}{q}+\psi_{\mathrm{BIOS}} \\ &\approx -\frac{Q_{\mathrm{s}}}{C_{\mathrm{ins}}}+\psi_{\mathrm{s}}+\frac{\varphi_{\mathrm{m}}-\varphi_{\mathrm{s}}}{q}-\chi^{\mathrm{sol}}+\psi_{\mathrm{c}}, \end{aligned} \tag{1}$$

where $V_{\rm GB}$ is the gate-body voltage, $Q_{\rm it}$ is the areal interface charge, $Q_{\rm f}$ is the areal fixed insulator charge, $C_{\rm ins}$ is the areal insulator capacitance, $\psi_{\rm s}$ is the surface potential, q is the elementary charge, and $\varphi_{\rm m}$, $\varphi_{\rm s}$ is the workfunction of the metal gate respectively semiconductor. In mature bulk CMOS technologies $Q_{\rm it}$ and $Q_{\rm f}$ can be neglected because of the relatively high induced total surface areal charge $Q_{\rm s}$. $\psi_{\rm BIOS}$ in Eq. (1) is the interfacial potential at the solution/insulator interface of which $\psi_{\rm c}$ is the chemical input parameter, shown to be a function of the solution pH, and $\chi^{\rm sol}$ is the surface dipole potential of the solvent. Note that for the potential of the reference electrode holds that $E_{\rm ref} = -V_{\rm GB} + \varphi_{\rm m}/q$, as originally proposed in [1].

Since the current in an ISBiT is governed by diffusion of minority charge, $Q_{\rm s}$ can be approximated by the areal depletion charge:

$$Q_{\rm d} \approx -\sqrt{2q\varepsilon_{\rm s}N_{\rm A}\psi_{\rm s}}, \tag{2}$$

where $N_{\rm A}$ is the substrate doping (acceptor) concentration and $\varepsilon_{\rm s}$ is the semiconductor permittivity.

After some manipulation with Eqs. (1)-(2) then for the surface potential can be derived (see [26] for a conventional MOSFET):

$$\psi_{\rm s} = \left(-\frac{\gamma}{2} + \sqrt{\frac{\gamma^2}{4} + V_{\rm GB} - \varphi_{\rm m} + \varphi_{\rm s} + \chi^{\rm sol} - \psi_{\rm c}}\right)^2, \tag{3}$$

with the body factor

$$\gamma = \frac{\sqrt{2\varepsilon_{\rm s}qN_{\rm A}}}{C_{\rm ins}}. \tag{4}$$

Eq. (3) indicates that the surface potential depends on both $V_{\rm GB}$ and the chemical input parameter that defines the sensor action. For deriving the relation between the $g_{\rm m}$ and sensitivity we first focus on deriving relations for the former.

For obtaining relations for $g_{\rm m}$ we need to describe relations for the current which is for an ISBiT more complicated than that for the ISFET. This is due to fact that for a low gate bias ($V_{\rm GS} < V_{\rm TH}$) a dominating bulk drain (or collector) current will spread across the p-type body caused by the internal bipolar transistor. The pn junction at the source side will then be forward biased causing an additional high carrier supply from the source (current flow (2) in Fig. 1(a)). In bulk FETs this is not the case because of the relatively low carrier injection from the source. In addition, for the same ISBiT operation mode the source current will be higher than the drain current because there will be a current flow between the source and the body/bulk, *i.e.* the body or base current of the bipolar transistor (current flow (3) in Fig. 1(b)). These additional current components hardly affect the $g_{\rm m}$ and as explained further in the text the sensitivity. From view point of power consumption these could be an issue. On the other hand, there are several ways to reduce these components among which employing fully-depleted silicon-on-insulator (FD-SOI) material.

The separate current components described above also determine an important figure-of-merit of the bipolar transistor: the common emitter current gain, or in short current gain, that is defined as being the ratio of the drain (or collector) current and the body (or base) current. In this work the current gain of the ISBiT has been studied as well.

To get into more detail, the drain current is governed by the channel length (or "base thickness"), the biasing (gate-body voltage $V_{\rm GB}$, body-source voltage $V_{\rm BS}$), and the substrate/body doping concentration. At low $V_{\rm GB}$ the drain diffusion current will mostly spread through the bulk channel region as indicated by the current flow lines (current flow (2) in Fig. 1(a)), while at high $V_{\rm GB}$ (superthreshold, strong inversion mode) the current will flow through path (1), *i.e.*, the traditional channel current. This current will then ultimately be determined by the channel resistance. The trend of reduced drain current spreading at high $V_{\rm GB}$ is confirmed by two-dimensional (2-D) TCAD simulations [27] shown in for example Fig. 2. There a zoom-in of the current flow line distribution of the drain current inside the ISBiT has been plotted for a fixed $V_{\rm BS}$ = 0.6 V and two different gate-body voltages: (a) $V_{\rm GB}$ = 0 V and (b) $V_{\rm GB}$ = 5.0V. For more details of the device parameters used in the simulations refer to section III.

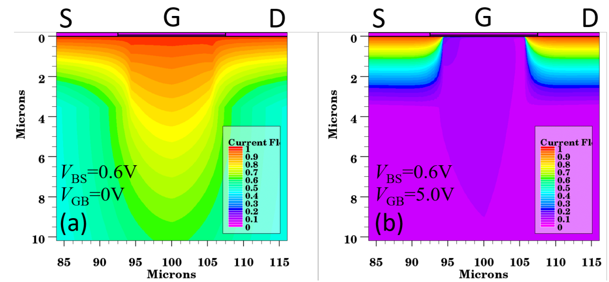

Fig. 2. Zoomed-in 2-D TCAD current flow simulations of the drain current in the channel region of the ISBiT for (a) $V_{\rm GB}$ = 0 V and (b) $V_{\rm GB}$ = 5.0V. For high $V_{\rm GB}$ there is less current spreading since practically most of the current flows via the channel. The body-source voltage $V_{\rm BS}$ = 0.6 V for both cases and gate length L = 15 μm. Further, same device parameters have been used as described in section III.

The body current on the other hand is governed by the source-body diode (current flow (3), Fig. 1(a)) and not by the gate. This diffusion current is the sum of two current components: (1) The hole component injected from the body region into the $\rm n^+$ source region diffusing to the source contact. In principle this component is inversely proportional to the implantation dose of the source region (or emitter Gummel number [28]), which is around $2{\cdot}10^{15}$ cm^{-2}. (2) the electron current injected from the source (emitter) in the body diffusing to the body contact. This component is inversely proportional to the dose of the diffused body contact plus the integral of the substrate doping from the source to the body contact in the third dimension. Since the body contact lies in the third dimension relatively far away from the (ISFET) active device (see Fig. 1(b)), which we did not include in our 2-D TCAD simulations, it is expected that the body current is mainly governed by the hole component. Therefore, the current gain is controlled by $V_{\rm GB}$ or the pH value as discussed in section III.

In [23], [24] physics-based models were reported for the drain current in the lateral gated bipolar transistor, showing

good agreement with TCAD simulations and experimental data. Partly because of the complexity of both models [23], [24], for understanding the difference between the operation of an ISFET and that of the ISBiT only some points of that work will be highlighted.

In the appendix a relation for the drain current I_D has been derived based on an alternative approach, from a view point of the bipolar transistor [25] rather than the MOSFET [24], where also a variation in doping or semiconducting materials in the body region has been assumed.

Assuming a uniform doping concentration and isotropic materials then from Eqs. (22), (23) we can summarize that (see appendix)

$$I_\mathrm{D} = I_0 \cdot e^{\frac{\psi_\mathrm{s}}{u_T}} e^{\frac{V_\mathrm{BS}}{u_T}} \left(1 - e^{-\frac{V_\mathrm{DS}}{u_T}}\right), \tag{5}$$

and

$$I_0 = \frac{qWD_\mathrm{n}}{L} \left(\frac{n_\mathrm{i}^2}{N_\mathrm{A}}\right) \cdot \int_0^\infty e^{\left(\frac{\psi(y)-\psi_\mathrm{s}}{u_T}\right)} dy. \tag{6}$$

where V_BS is the body-source voltage and V_BD is the body-drain voltage.

This relation includes both the bulk drain current and the (surface) drain current of the ISBiT. For more realistic cases the infinity ("∞") symbol in the integral can be replaced by x_j, *i.e.* the drain- and source-body junction depth (as suggested by [23]). This integral, that depends on ψ_s, can only be solved numerically. However, at a high gate bias the current at the semiconductor surface is dominant. Basically, the bulk drain current can then be ignored and the integral can be replaced by the term $u_T C_\mathrm{d}/(qN_\mathrm{A})$, with C_d is the areal depletion capacitance [26].

Once at low V_GS for $V_\mathrm{BS} = 0$ V, Eq. (5) reduces to the traditional subthreshold drain current of the ISFET. Hence, for the same device geometry the ISBiT has a much higher current than the ISFET because of the (positive) exponential term formed by V_BS yielding an increased electron injection when operating it in forward active mode (V_BS >0 V, V_BD $\leq$0 V). In other words, a positive V_BS literally reduces the threshold voltage of the device.

Consequently, for strong inversion operation [22], [1] when the bulk drain current is less important it can be stated that

$$I_\mathrm{D} = \mu_\mathrm{n} C_\mathrm{ins} \frac{W}{L} \cdot \left(V_\mathrm{GB} - (V_\mathrm{TH} - V_\mathrm{BS}) - \frac{V_\mathrm{DS}}{2}\right) V_\mathrm{DS}, \tag{7}$$

when operating the device in linear mode ($V_\mathrm{GD} > V_\mathrm{TH}$) and

$$I_\mathrm{D} = \mu_\mathrm{n} C_\mathrm{ins} \frac{W}{2L} \cdot (V_\mathrm{GB} - (V_\mathrm{TH} - V_\mathrm{BS}))^2, \tag{8}$$

for the saturation mode ($V_\mathrm{GD} \leq V_\mathrm{TH}$).

For the threshold voltage can be written [1]:

$$V_\mathrm{TH} = -\frac{Q_\mathrm{d}}{C_\mathrm{ins}} + 2\varphi_\mathrm{b} + \frac{\varphi_\mathrm{m} - \varphi_\mathrm{s}}{q} - \chi^\mathrm{sol} + \psi_\mathrm{c}, \tag{9}$$

with φ_b is the built-in potential of the depleted silicon.

The transconductance is defined as

$$g_\mathrm{m} = \frac{\partial I_\mathrm{D}}{\partial V_\mathrm{GB}} = \frac{\partial I_\mathrm{D}}{\partial \psi_\mathrm{s}} \cdot \frac{\partial \psi_\mathrm{s}}{\partial V_\mathrm{GB}}, \tag{10}$$

and is per definition governed by the variation of V_GB.

Therefore, the following relation can be derived for the subthreshold operation using Eqs. (3)-(5)

$$g_\mathrm{m} = \frac{I_\mathrm{D}}{u_T} \cdot \frac{C_\mathrm{ins} + C_\mathrm{d}}{C_\mathrm{ins}} = \frac{I_\mathrm{D}}{u_T} \cdot m, \tag{11}$$

with

$$C_\mathrm{d} = \frac{\partial Q_\mathrm{d}}{\partial \psi_\mathrm{s}} = \frac{\gamma C_\mathrm{ins}}{2\sqrt{\psi_\mathrm{s}}} \tag{12}$$

and m is the ideality factor. The latter should preferably be unity, but obviously because of the presence of C_d m >1. At subthreshold I_D increases exponentially by the additional electron injection in the ISBiT. As a result, g_m is the highest here for the ISBiT and increases with V_BS.

Further, at strong inversion holds that [22]

$$g_\mathrm{m} = \mu_\mathrm{n} C_\mathrm{ins} \frac{W}{L} V_\mathrm{DS}, \tag{13}$$

in linear mode (obtained from Eq. (8)), while in saturation mode (obtained from Eq. (10))

$$g_\mathrm{m} = \mu_\mathrm{n} C_\mathrm{ins} \frac{W}{L} \cdot (V_\mathrm{GB} - (V_\mathrm{TH} - V_\mathrm{BS})). \tag{14}$$

From the discussion above it can be summarized that the transconductance of the ISBiT

- will exponentially increase with V_BS at subthreshold,
- will not change in linear mode, and
- will linearly increase with V_BS in saturation mode.

Finally, we also would like to know the impact of the device on the pH-sensitivity, an important measure for the sensor. It can be derived that [2]

$$\frac{\partial \psi_\mathrm{c}}{\partial \mathrm{pH}} = -2.3 u_T \alpha. \tag{15}$$

α is a dimensionless sensitivity parameter depending on the aqueous solution:

$$\alpha = \frac{1}{\frac{2.3 u_T C_\mathrm{dif}}{q\beta_\mathrm{int}} + 1}, \tag{16}$$

where β_int is the intrinsic buffer capacity, of the oxide surface and C_dif is the differential double-layer capacitance. β_int is determined by three material parameters at the oxide: the acid and base equilibrium constants of the amphoteric oxide surface groups and the total density of available surface sites. Further, C_dif is defined as the first derivative of the surface charge with ψ_c.

For ideal operation α = 1 hence $\frac{\partial \psi_\mathrm{c}}{\partial \mathrm{pH}} \approx$ -59.2 mV/pH at room temperature, *i.e.* the Nernstian sensitivity [2].

Since Eq. (1) basically holds for the whole device operating range, it can be generally stated that ($\frac{\partial V_\mathrm{GB}}{\partial \psi_\mathrm{c}} = 1$)

$$\frac{\partial I_\mathrm{D}}{\partial \mathrm{pH}} = \frac{\partial I_\mathrm{D}}{\partial V_\mathrm{GB}} \cdot \frac{\partial V_\mathrm{GB}}{\partial \psi_\mathrm{c}} \cdot \frac{\partial \psi_\mathrm{c}}{\partial \mathrm{pH}} = g_\mathrm{m} \cdot \frac{\partial \psi_\mathrm{c}}{\partial \mathrm{pH}} = -2.3 u_T \alpha \cdot g_\mathrm{m}. \tag{17}$$

In other words, for increasing the sensitivity of the biosensor, the transconductance should be maximized and α should be unity.

III. Results

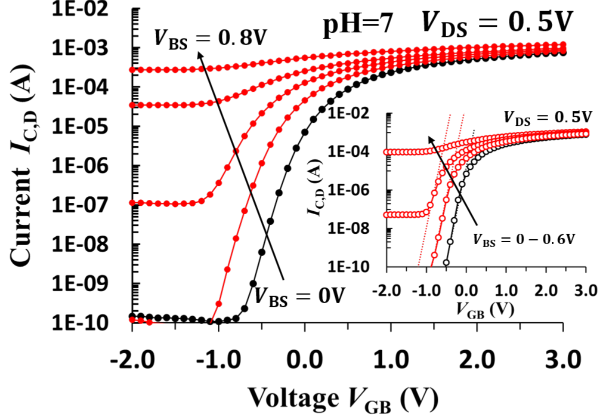

Fig. 3. Measured I_D-V_{GB} curves of the sensor for pH=7 (V_{DS} = 0.5 V). The inset shows TCAD simulation data for the same device along with the subthreshold current model (Eq. (5)).

The schematic cross-section of the device under study is depicted in Fig. 1(a). The gate stack comprises a 70 nm thick thermal silicon-dioxide (SiO_2) layer and a 120 nm thick tantalum-oxide (Ta_2O_5) layer for improving the sensitivity [1]. The gate length L and width W are 15 respectively 500 μm. A separate body or bulk contact is used for forward biasing the source-body diode and therefore the bipolar transistor. Fig. 1(b) shows the top view layout of the completed device where all direct electrical connections (body, source and drain) are placed on top. Except for the part with the connections, during the measurements the structure was dipped in a glass beaker containing an aqueous solution for further investigation.

For the aqueous solution the pH was varied between 4.01, 7 and 10.01, by using standard buffer solutions (provided by Radiometer analytical). Further, the whole system containing the beaker and sensor was placed in a shielded and dark environment. For each pH value the I_D-V_{GS} characteristics were measured.

Fig. 3 shows the I_D-V_{GS} characteristics for pH = 7. The first thing noticeable is that the I_D increases for higher V_{BS}. As discussed in section II, a positive V_{BS} exponentially increases the subthreshold current and linearly increases the current at strong inversion. In addition, once in saturation mode (V_{DB}=5 V) the I_D shows a quadratic increase with V_{BS} (not shown), as expected from the theory. Clearly, the ISBiT operation seems to be more attractive from this view point.

However, as can be seen, constant current plateaus are formed for low V_{GB} and these increase for higher V_{BS}. These plateaus originate from the bulk drain current (flow (2), Fig. 1(a)). The same trend was observed for the source current, though these plateaus were higher because of the additional large bulk current component from the source-body diode (*i.e.*, base current flow (3), Fig. 1(a)). As will be shown, those plateaus are not essential for the sensitivity but could be important from view point of power consumption.

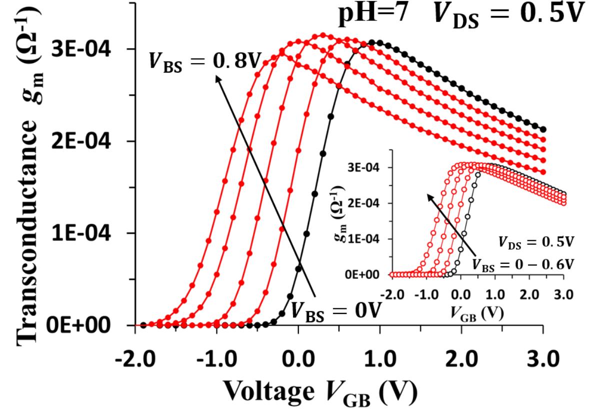

Fig. 4. Measured g_m-V_{GB} curves of the sensor for pH=7 (V_{DS} = 0.5 V). The inset shows TCAD simulation data for the same device.

TCAD simulations [27] were performed (Fig. 3, inset) showing good agreement with the experimental data. Because for the pH=7 case similar electrical results were obtained with our dry measurements we adopted an aluminum gate with a work function (φ_m) of 4.1 eV (as taken default for Atlas, Silvaco) and implemented at the Si/SiO_2 interface a fixed areal charge density of 10^{11} cm^{-2}. Even though not being part of this work, for emulating pH variation in TCAD adjusting this fixed charge density would be a good direction. For completeness sake in Fig. 3 (inset) the simple subthreshold model (Eq. (5)) has been plotted along with TCAD data where only I_0 has been fitted. The trend that V_{BS} exponentially increases the subthreshold current, hence reduces V_{TH} is also visible.

From the I_D-V_{GB} curves shown in Fig. 3 the g_m has been determined, see Fig. 4. As discussed in section II, the g_m increases with V_{BS} when operating the device below or near V_{TH}. However, the results also show that g_m drops for higher V_{GB} and this drop becomes stronger for high V_{BS} as well. This effect can be explained by the gate field-induced mobility reduction (not taken into account in Eq. (13)): the vertical field increases particularly close the source region because of the high V_{GS}. Therefore, in the linear mode operation (above V_{TH}) the g_m of the ISBiT is less than that of the ISFET. An optimum g_m has been obtained at V_{BS} $\approx$ 0.4 V because of the counteracting effects formed by the mobility reduction and the increase of electron injection both tuned by V_{BS}.

For confirmation the g_m has been extracted from TCAD simulation data as well, showing the same trend (inset, Fig. 4).

Fig. 5 shows the g_m when operating the device in saturation mode (V_{DB} = 5.0 V, pH = 7). The results show that indeed the g_m increases with V_{BS}, simply because of the V_{TH} reduction. However, the g_m-V_{GB} curves do not show a linear increase as described in Eq. (14), which is also due to some field-induced mobility reduction effects. Further, like before TCAD simulations show the same trend, see inset of Fig. 5.

We also investigated the pH-sensitivity of the device. Fig. 6 shows the extracted reference voltage, V_{GB}, against the pH of

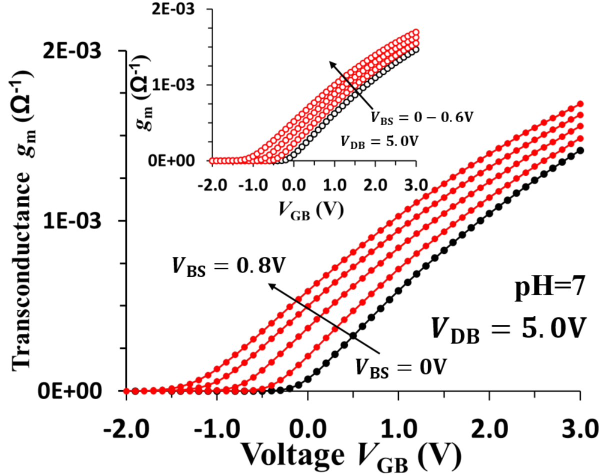

Fig. 5. Measured g_m-V_{GB} curves of the sensor for pH=7 (V_{DB} = 5.0 V). The inset shows TCAD simulation data for the same device.

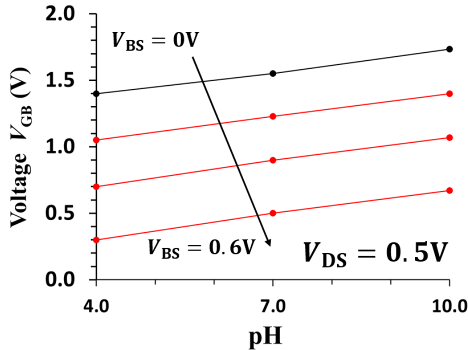

Fig. 6. Measured reference voltage (V_{GB}) against the pH for various V_{BS} (V_{DS} = 0.5 V).

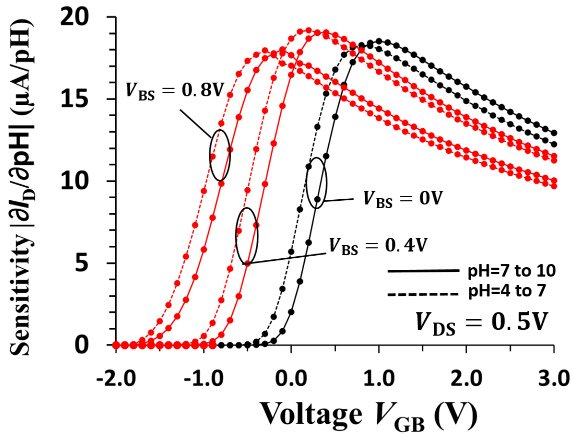

Fig. 7. Measured absolute pH-sensitivity ($|\frac{\partial I_D}{\partial pH}|$) against V_{GB} for V_{BS}=0, 0.4, and 0.8 V in the linear operation mode (V_{DS} = 0.5 V). For these values the measured I_D data were obtained for the change from pH=4.01 to 7 and from pH=7 to 10.01.

the aqueous solution for various V_{BS} when operating the device in linear mode. The results show approximately the same slope for various V_{BS}: $\frac{\partial V_{GB}}{\partial pH}$ $\approx$ 58.3$\pm$ 0.5 mV/pH, and this value hardly changed for other operation modes. The reason for this is that this slope is governed by the pH of the aqueous solution

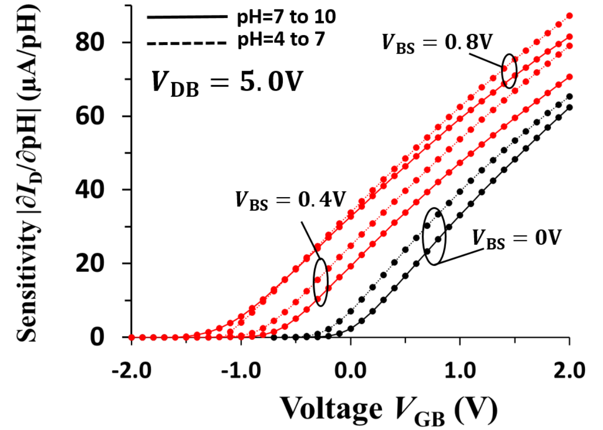

Fig. 8. Measured absolute pH-sensitivity ($|\frac{\partial I_D}{\partial pH}|$) against V_{GB} for V_{BS}=0, 0.4, and 0.8 V in the saturation operation mode (V_{DB} = 5.0 V). For these values the measured I_D data were obtained for the change from pH=4.01 to 7 and from pH=7 to 10.01.

rather than by the device (transducer).

We also investigated the effect of the pH on the I_D for different modes of operation, see Figs. 7 and 8. For this we varied the pH from 4.01 to 7, extracted the ΔI_D from that, and in turn determined the pH sensitivity ($\frac{\partial I_D}{\partial pH}$) from that. The same was done for the pH change from 7 to 10.01.

The $\frac{\partial I_D}{\partial pH}$-$V_{GB}$ curves show the same trend as the g_m-V_{GB} curves (Figs. 4 resp. 5) as predicted from Eq. (15). From the data an α $\approx$ 0.98 was obtained in linear operation mode.

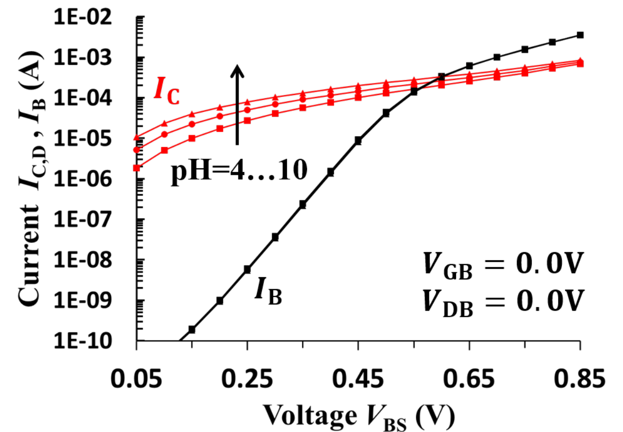

Fig. 9. Measured drain and body (base) currents of the sensor against V_{BS} for various pH values (4.01, 7, and 10.01) (V_{DB} = V_{GB} = 0.0 V).

Finally, we studied the current gain behavior of the ISBiT. Fig. 9 shows the drain and body current against V_{BS} by varying the source potential for the three pH values used before: 4.01, 7, and 10.01. The drain, gate, and body potential were grounded here. The results indicate a weaker slope for the drain current then for the body current. This can be explained by the fact that the gate bias dependent drain current is then near strong inversion (V_{GB} >0 V) and hence is governed by the channel resistance (estimated to be around 2kΩ), where the mobility reduction plays a role. The body current on the other hand is determined by the source-body diode as discussed

in section II. This current exponentially increases with V_{BS} and flows independently from the gate bias. This can also be observed in the pH dependence of both current components: the body current is not affected by the pH value, though the drain current is, as discussed before. Consequently, because of different dependencies for each current component the current gain reduces for high V_{BS}.

The latter can also be confirmed during the operation of the ISBiT by applying a V_{GB} bias for various V_{BS} (pH = 7, V_{DB} = 5.0 V) as shown in Fig. 10. Maximum current gain values drop in the range of $\sim 10^4$ to less than unity when increasing V_{BS} from 0.4 V to 0.8 V. The high current gain at low V_{BS} can be explained by the relatively high dose source region compared to the gated lowly doped channel region. For a low gate bias however there are hardly any differences since then the drain current is mostly diffusing through the bulk channel region as discussed in section II, refer to Fig. 1(a) (current flow (2)) and *e.g.* Fig. 2(a).

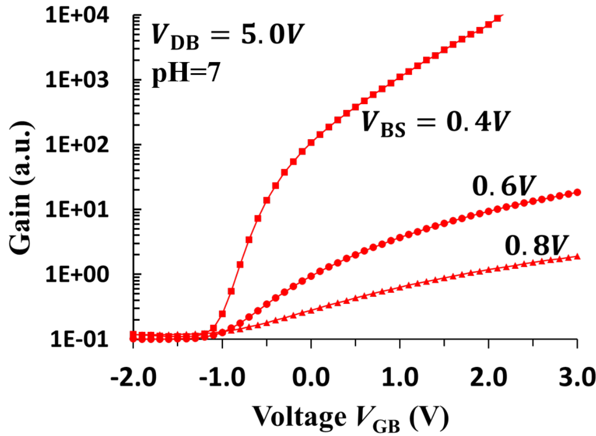

Fig. 10. Measured current gain of the sensor against V_{GB} for V_{BS} = 0.4, 0.6 and 0.8 V (pH=7, V_{DB} = 5.0 V).

IV. Conclusions

The ion-sensitive field-effect transistor has been studied by forward biasing the source-body diode. As a result, a gated bipolar transistor has been switched on, also referred to as the ion-sensitive bipolar transistor (ISBiT). The ISBiT operates at a lower gate voltage with a higher transconductance in sub- and near threshold compared to the ISFET. However, because of the field-induced mobility-reduction effect it shows a lower transconductance in the linear mode operation (above threshold). Maximum transconductances have been obtained for the former when operating the sensor in saturation mode. The same trends have been obtained for the pH-sensitivity because of a direct relation with the transconductance, as predicted by theory.

The fact that the sensitivity can be tuned by simply adjusting the body bias within the same ISFET technology, makes the ISBiT an interesting sensor concept.

V. Appendix

For the collector current of a bipolar transistor the following relation holds [25]:

$$I_C = I_{sat} \cdot \left(e^{\frac{V_{BE}}{u_T}} - e^{\frac{V_{BC}}{u_T}} \right), \tag{18}$$

where V_{BE} is the base-emitter voltage, V_{BC} is the base-collector voltage, and the saturation current

$$I_{sat} = \frac{q n_i^2 W}{G_B} = \frac{q n_i^2 W}{\int_0^L \left(\int_0^\infty \left(\frac{n_{ie}(x,y)}{n_i} \right)^2 \cdot \left(\frac{D_n(x,y)}{p(x,y)} \right) dy \right)^{-1} dx}. \tag{19}$$

n_{ie} is the doping and material (composition) dependent intrinsic carrier concentration and W is the gate or base width. G_B is the Gummel number of the body that originally was proposed in [25], and re-formulated in [28].

The hole concentration, which is affected by the surface potential hence V_{GB}, in turn can be described as

$$p(x,y) = N_A(x,y) \cdot e^{\left(-\frac{\psi(x,y)}{u_T} \right)}, \tag{20}$$

where ψ is the electrostatic potential in the semiconductor described as:

$$\psi(x,y) = \frac{q N_A(x,y)}{\varepsilon_s} \cdot \frac{y^2}{2} - \frac{\sqrt{2 q N_A(x,y) \varepsilon_s \psi_s(x)}}{\varepsilon_s} \cdot y + \psi_s(x). \tag{21}$$

When we consider no variation in doping or material composition in the body then we can simplify the above relations. Then after some rewriting we obtain

$$I_C = I_0 \cdot e^{\frac{\psi_s}{u_T}} \left(e^{\frac{V_{BE}}{u_T}} - e^{\frac{V_{BC}}{u_T}} \right), \tag{22}$$

and

$$I_0 = \frac{q W D_n}{L} \left(\frac{n_i^2}{N_A} \right) \cdot \int_0^\infty e^{\left(\frac{\psi(y) - \psi_s}{u_T} \right)} dy. \tag{23}$$

References

[1] P. Bergveld, “Thirty years of ISFETOLOGY: What happened in the past 30 years and what may happen in the next 30 years”, *Sensors and Actuators B: Chemical*, vol. 88, no. 1, pp. 1-20, 2003.

[2] W. Olthuis, “Chemical and physical FET-based sensors or variations on an equation”, *Sensors and Actuators B*, vol. 105, pp. 96-103, 2005.

[3] C. Cané, I. Gràcia, and A. Merlos, “Microtechnologies for pH ISFET chemical sensors”, *Microelectronics Journal*, vol. 28 (4 SPEC. ISS.), pp. 389-405, 1997.

[4] Y.-L. Chin, J.-C. Chou, T.-P. Sun, H.-K. Liao, W.-Y. Chung, and S.-K. Hsiung, “A novel SnO_2/Al discrete gate ISFET pH sensor with CMOS standard process”, *Sensors and Actuators, B: Chemical*, vol. 75, no. 1-2, pp. 36-42, 2001.

[5] S. Nakata, T. Arie, S. Akita, and K. Takei, “Wearable, Flexible, and Multifunctional Healthcare Device with an ISFET Chemical Sensor for Simultaneous Sweat pH and Skin Temperature Monitoring”, *ACS Sensors*, vol. 2, no. 3, pp. 443-448, 2017.

[6] X. Huang, H. Yu, X. Liu, Y. Jiang, M. Yan, and D. Wu, “A Dual-Mode Large-Arrayed CMOS ISFET Sensor for Accurate and High-Throughput pH Sensing in Biomedical Diagnosis”, *IEEE Transactions on Biomedical Engineering*, vol. 62, no. 9, art. no. 7078866, pp. 2224-2233, 2015.

[7] P.L.H.M. Cobben, R.J.M. Egberink, J.G. Bomer, P. Bergveld, W. Verboom, and D.N. Reinhoudt, “Transduction of Selective Recognition of Heavy Metal Ions by Chemically Modified Field Effect Transistors (CHEMFETs)”, *J. Am. Chem. Soc.*, vol. 114, no. 26, pp. 10573-10582, 1992.

[8] J. Janata, “Thirty years of CHEMFETs - A personal view”, *Electroanalysis*, vol. 16, no. 22, pp. 1831-1835, 2004.

[9] F. Davis, S.D. Collyer, and S.P.J. Higson, “The construction and operation of anion sensors: Current status and future perspectives”, *Topics in Current Chemistry*, vol. 255, pp. 97-124, 2005.

[10] S.-R. Chang and H. Chen, “A CMOS-compatible, low-noise ISFET based on high-efficiency ion-modulated lateral-bipolar conduction”, *Sensors*, vol. 9, pp. 8336-8348, 2009.

[11] C.-Y. Chen, H.-L. Hsieh, T.-P. Sun, C.T.-S. Ching, and P.-L. Liu, “Extended base H+-ion sensitive bipolar junction transistor with SnO_2/ITO glass sensing membrane”, *IEEE Sensors*, pp. 1113-1116, 2009.

[12] T.-P. Sun, H.-L. Shieh, C.-L. Liu, and C.-Y. Chen, “Urea biosensor based on an extended-base bipolar junction transistor”, *Bio-Medical Materials and Eng.*, vol. 24, pp. 21-28, 2014.

[13] D. Zhang, X. Gao, S. Chen, H. Norström, U. Smith, P. Solomon, S.-L. Zhang, and Z. Zhang, “An ion-gated bipolar amplifier for ion sensing with enhanced signal and improved noise performance”, *Appl. Phys. Lett.*, vol. 105, p. 082102, 2014.

[14] S. Zafar, M. Khater, V. Jain, and T. Ning, “A comparison between bipolar transistor and nanowire field effect transistor biosensors”, *Appl. Phys. Lett.*, vol. 106, p. 063701, 2015.

[15] S. Zafar and T. Ning, “Bipolar junction transistor based sensors for chemical and biological sensing”, *ESSDERC*, pp. 389-392, 2016.

[16] S. Verdonckt-Vandebroek, S.S. Wong, J.C.S. Woo, and P.K. Ko, “High-Gain Lateral Bipolar Action in a MOSFET Structure”, *IEEE Trans. Electr. Dev.*, vol. 38, no. 11, pp. 2487-2496, 1991.

[17] S. Verdonckt-Vandebroek, J.H. You, J.C.S. Woo, and S.S. Wong, “High Gain Lateral P-N-P Bipolar Action in a p-MOSFET Structure”, *IEEE Electr. Dev. Lett.*, vol. 13, no. 6, pp. 312-313, 1992.

[18] F. Assaderaghi, D. Sinitsky, S. Parke, J. Bokor, P.K. Ko, and C. Hu, “A dynamic threshold voltage MOSFET (DTMOST) for ultra-low voltage operation”, *IEDM*, pp. 809-812, 1994.

[19] D.A. Sunderland, S.-J. Jeng, D. Nguyen-Ngoc, B. Martin, E.C. Eld, T. Tewksbury, D.C. Ahlgren, M.M. Gilbert, J.C. Malinowski, K.T. Schonenberg, K.J. Stein, B.S. Meyerson, and D.L. Harame, “Gate-Assisted Lateral PNP Active Load for Analog SiGe HBT Technology”, *BCTM*, pp. 23-26, 1996.

[20] H. Yuan, H.-C. Kwon, S.-H. Yeom, D.-H. Kwon, and S.-W. Kang, “MOSFET-BJT hybrid mode of the gated lateral bipolar junction transistor for C-reactive protein detection”, *Biosensors and Bioelectronics*, vol. 28, pp. 434-437, 2011.

[21] H. Yuan, J.-X. Zhang, C. Zhang, N. Zhang, L.-X. Xu, M. Ding, and P.J. Clarke, “Low Gate Voltage Operated Multi-emitter-dot H+ Ion-Sensitive Gated Lateral Bipolar Junction Transistor”, *Chin. Phys. Lett.*, vol. 32, no. 2, p. 020701, 2015.

[22] S.M. Sze and K.K. Ng, “Physics of Semiconductor Devices”, 3rd edition, John Wiley & Sons, Inc., USA, 2007.

[23] K. Joardar, “An improved analytical model for collector currents in lateral bipolar transistors”, *IEEE Trans. Electr. Dev.*, vol. 41, no. 3, pp. 373-382, 1994.

[24] W.R. McKinnnon, R. Ferguson, and S.P. McAlister, “A model for gated-lateral BJT’s based on standard MOSFET models”, *IEEE Trans. Electr. Dev.*, vol. 46, no. 2, pp. 427-429, 1999.

[25] H.K. Gummel and H.C. Poon, “An Integral Charge Control Model of Bipolar Transistors”, *Bell Syst. Techn. J.*, vol. 49, p. 827, 1970.

[26] N. Arora, “MOSFET MODELING FOR VLSI SIMULATION: Theory and Practice”, *World Scientific Co. Pte. Ltd.*, 2007.

[27] *Atlas device simulation software, version 5.25.2.C*, Silvaco, Inc., Santa Clara, USA, 2017.

[28] J.W. Slotboom, “Analysis of Bipolar Transistors”, *PhD thesis*, Eindhoven University of Technology, Eindhoven, Oct. 1977.